A Fully Electronic DNA Sensor With 128 Positions and In-Pixel A/D Conversion

Meinrad Schienle, Christian Paulus, Alexander Frey, Franz Hofmann, Birgit Holzapfl, Petra Schindler-Bauer, and Roland Thewes, *Member, IEEE*

Abstract—A 16 \times 8 sensor array chip for fully electronic DNA detection is presented. The sensor principle is based on an electrochemical redox cycling process. The chip is fabricated on the basis of an extended 0.5 μ m CMOS process. Each sensor site of the array chip contains a complete A/D converter with a dynamic range of five decades. The 3σ -homogeneity of the electrical response of the sensor array is better than 6% (10^{-11} A to 10^{-7} A) and better than 20% (10^{-12} A to 10^{-7} A). Proper operation of the chip is demonstrated with electrochemical and biological experiments.

Index Terms—DNA, electrochemical devices, chemical transducers, CMOS integrated circuits, current measurement, drugs, microelectrodes.

I. INTRODUCTION

N MANY FIELDS of biotechnology, tools are required to detect the presence or absence of specific DNA sequences in a given sample. The development of DNA microarrays in recent years has opened the way to high parallelism and high throughput [1]–[7]. The most widely known applications are genome research and drug development. The realization of fully electronic medium-density DNA sensor array chips [8]–[10] is attracting increasing interest for diagnostic purposes. Such electronic approaches avoid expensive optical set-ups used in today's commercially available systems based on optical readout methods; they promise ease of use and robust applicability. However, the status of development of today's electronic systems is lower compared to optical systems.

Recently, a fully electronic DNA sensor array with 128 sensor positions was presented based on an electrochemical detection principle [9], [11]. There, each sensor pixel consists of a circuit which controls the electrode voltages and provides a 100-fold value of the sensor currents at the pixel output. Analog data transmission within the whole array circuit is required.

Using the same detection principle as in [9] and [11], in this paper we report on a new DNA sensor array chip with analog-to-digital (A/D) conversion realized within each pixel [12]. This approach provides a high dynamic range of five decades and is well suited as a robust platform to measure transducer-generated currents within a wide range of applications.

This paper is organized as follows. In Sections II and III, brief introductions are given concerning the operation of DNA microarrays in general, and the redox-cycling detection method used here. In Section IV, the design of the circuits for the realization of active sensor sites with in-sensor site A/D conversion

is discussed. In Section V, first the results of the electrical characterization of the chip are presented. Then, the proper operation of the full system is demonstrated by the results of electrochemical and biological measurements. Finally, in Section VI, the paper is summarized.

II. BASIC OPERATION PRINCIPLE OF DNA MICROARRAYS

The purpose of DNA microarrays is to enable the parallel investigation of a given sample concerning the presence of specific DNA sequences. Depending on the application, requirements range from relatively simple "presence or absence" investigations to quantitative analyses with a high dynamic range.

In general, a DNA microarray chip is a slide made of glass, a polymer material, silicon, etc. On the surface of such a chip, single-stranded DNA receptor molecules ("probes") are immobilized at predefined positions [Fig. 1(a)]. These probe molecules consist of different DNA sequences of typically 20 to 40 bases. Whereas a number of different techniques are known to functionalize the chips [13]–[17], in our case off-chip synthesized probe molecules are deposited on the surface of the chips using a microspotter [13].

In Fig. 1(b) and (c), two different sites within an array are considered after the immobilization phase. For simplicity, only five bases are drawn in this schematic illustration. As shown in Fig. 1(d) and (e), in the next step the whole chip is flooded with a sample containing the target molecules. In case of complementary DNA sequences of probe and target molecules, their match leads to hybridization [Fig. 1(d)]. If probe and target molecules mismatch, this chemical binding process does not occur [Fig. 1(e)]. After a washing step, double-stranded DNA is obtained only at the matching positions [Fig. 1(f)]. At the mismatch sites single-stranded DNA molecules remain, and the same situation as in the initial case shown in Fig. 1(c) is reached again. Since the receptor molecules are known, the information, whether double- or single-stranded DNA is found at different test sites, reveals the composition of the sample. Thus, the requirement remains to identify the sites with double-stranded DNA. In today's commercially available systems, the target molecules are usually labeled with fluorescence markers molecules and an optical image of the array chip reveals the positions with double-stranded DNA [1]–[7].

III. REDOX-CYCLING DETECTION METHOD

The electrochemical sensor principle used here is based on an electrochemical redox-cycling technique [11], [18]–[20].

Manuscript received April 30, 2004; revised July 10, 2004.
The authors are with Infineon Technologies AG, Corporate Research,
D-81730 Munich, Germany (e-mail: meinrad.schienle@infineon.com).
Digital Object Identifier 10.1109/JSSC.2004.837084

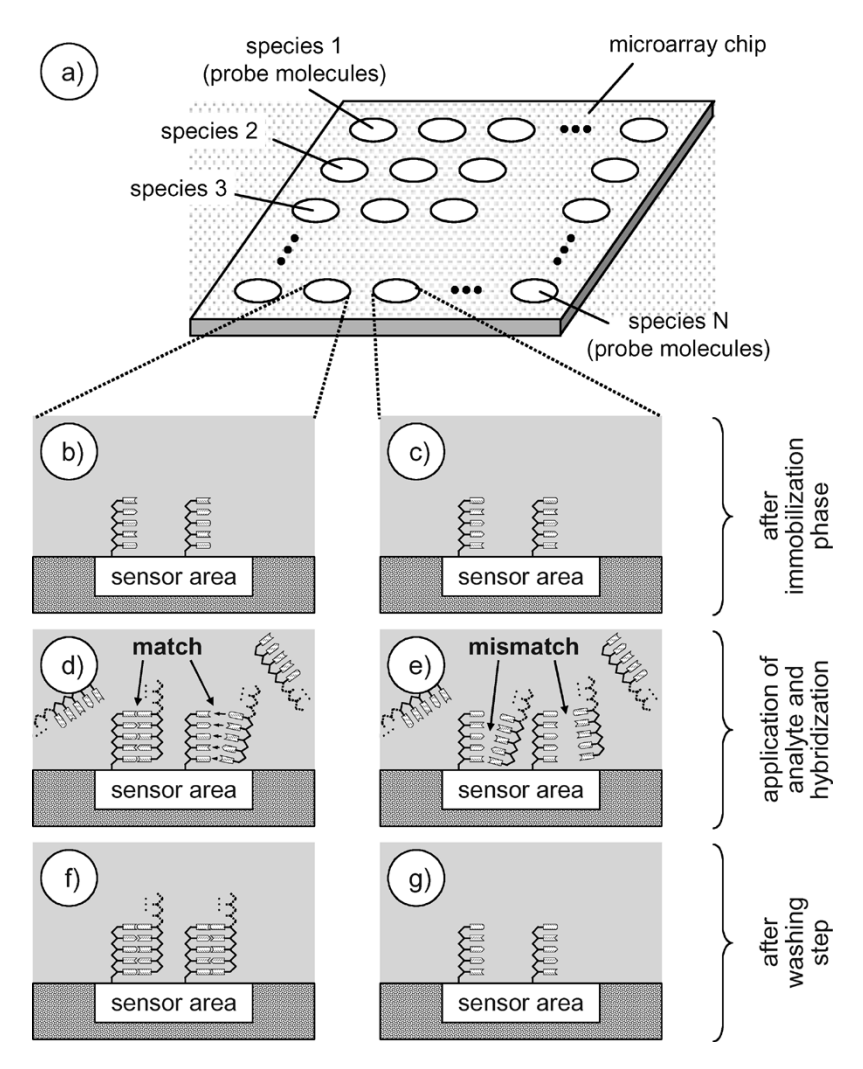


Fig. 1. (a) Schematic plot of a DNA microarray chip. (b)–(g): Schematic consideration of two different test sites. The left column (b), (d), (f) shows the case of matching molecules; the right column (c), (e), (g) shows the case of mismatching target molecules.

A single sensor site (Fig. 2, left) consists of interdigitated gold electrodes (generator and collector electrode) with width = spacing = 1 μ m. Probe molecules are immobilized on the gold surface (e.g., by thiol coupling). The target molecules in the sample are tagged by an enzyme label (alkaline phosphatase). After hybridization and washing phases, a chemical substrate (para-aminophenylphosphate) is applied to the chip. At the position with matching DNA strands the enzyme label cleaves the phosphate group and generates an electrochemically active compound (para-aminophenol) (Fig. 2, right). Applying simultaneously an oxidation and a reduction potential to the sensor electrodes ($V_{\rm gen}$ and $V_{\rm col}$, e.g., +200 mV and -200 mV with respect to the on-chip reference potential), para-aminophenol is oxidized to quinoneimine at the generator electrode, and quinoneimine is reduced to para-aminophenol at the collector electrode. In this way currents are generated at the electrodes ($I_{\rm gen}$ and $I_{\rm col}$). Since not all particles oxidized at the generator reach the collector electrode, a regulated four electrode system is used. A potentiostat, whose input and output are connected to a reference and to a counter electrode, respectively, provides the difference current to the electrolyte and regulates the potential of the electrolyte to a constant value. The current flow at the sensor electrodes has two contributions,

firstly the current initially generated by the enzyme label, and secondly the current of the redox-cycling at the sensor electrodes. Moreover, due to electrochemical artifacts an offset current may contribute to the detection current as well, so that usually the derivatives of the sensor current with respect to the measurement time, $\partial I_{\rm col}/\partial t$ and $\partial I_{\rm gen}/\partial t$, are evaluated instead of the absolute values. A more detailed discussion of this method is given elsewhere [11], [18]–[20].

IV. CHIP DESIGN

Fig. 3 shows the principle of the in-pixel A/D conversion. The voltage of the sensor electrode is controlled by a regulation loop via an operational amplifier and a source-follower transistor. For A/D conversion, a current-to-frequency converting sawtooth generator concept is used. Similar concepts have been proposed in the area of image sensors [21]–[24]. The sensor current charges an integrating capacitor $C_{\rm int}$. When the switching level of the comparator is reached, a reset pulse is generated which passes through the delay stage and the capacitor is discharged by transistor $M_{\rm res}$ again. The delay stage is required as a pulse shaping unit to ensure a sufficient length of the reset

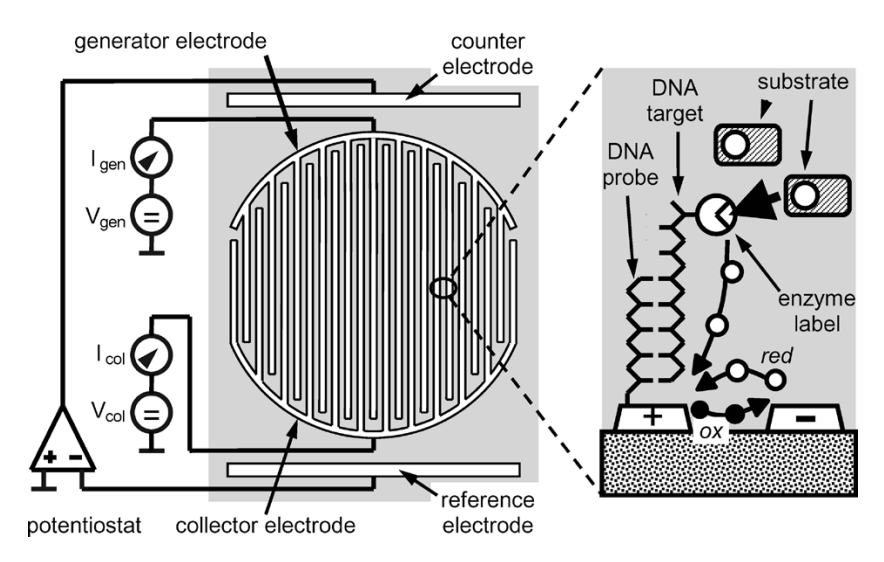


Fig. 2. Left: schematic plot of the electrode configuration. Right: schematic illustration of the redox-cycling process.

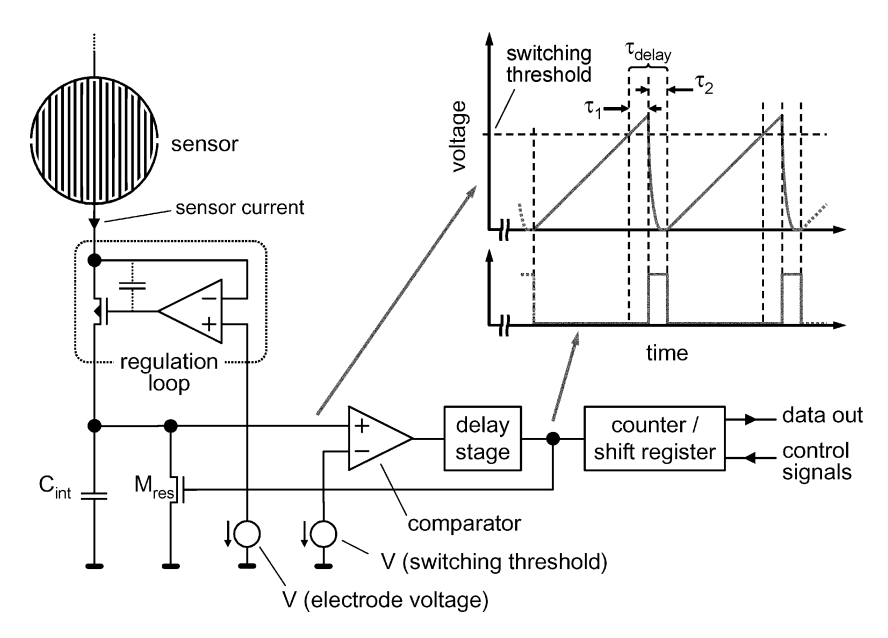


Fig. 3. Principle for A/D conversion of the sensor current.

pulse applied to $M_{\rm res}$ so that complete discharging of the integrating capacitor is guaranteed. The number of reset pulses is counted for a given time interval with a digital counter. With this free-running oscillator concept, the data from all sites are sampled simultaneously without the need for a complicated timing scheme.

In Fig. 4, two different comparator circuit designs are depicted used for the generator branch. For the collector electrode, complementary designs are used. Both comparators are based on a Miller-type opamp. They differ in the reset pulse-shaping circuit. The first design (type A) uses an inverter chain as a delay line. The second design (type B) uses a flip-flop which provides a built-in hysteresis.

The frequency behavior as a function of the sensor current including parasitic and device mismatch effects is described by the following equation:

$$1/f = \frac{(V_{\text{sw}} + V_{\text{offset}}) \times C}{I_{\text{electrode}} + I_{\text{leak}}} + \tau_{\text{delay}}$$
 (1)

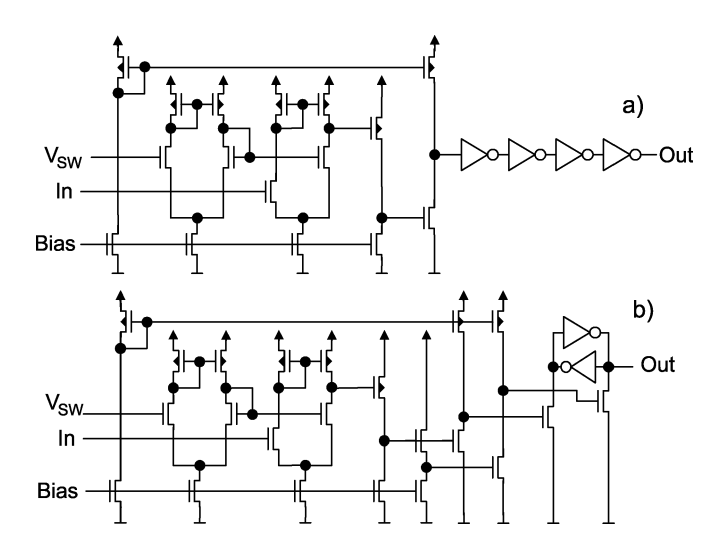


Fig. 4. Comparator circuits. (a): Pulse shaping by inverter chain (type A). (b): Pulse shaping with flip-flop (type B).

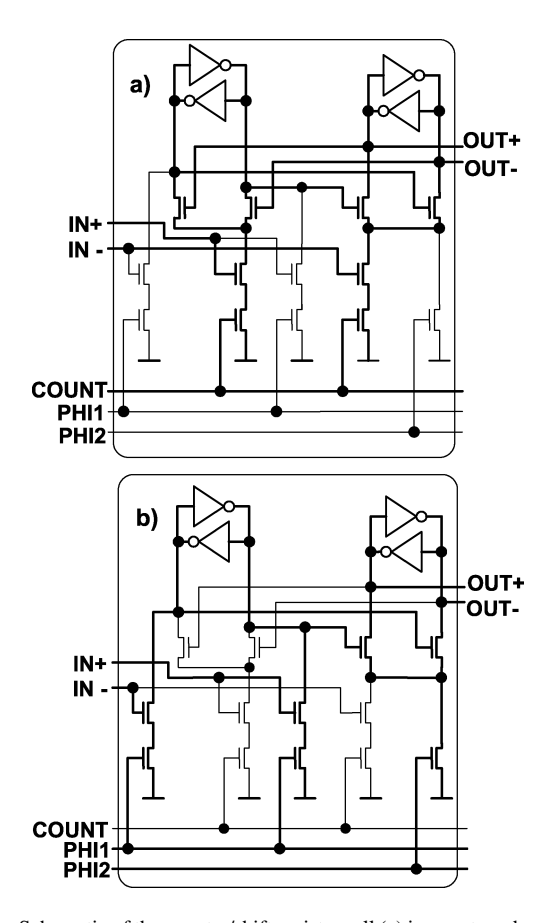


Fig. 5. Schematic of the counter/shift register cell (a) in count mode and (b) in shift mode. Inactive signals are drawn with thin lines.

where f is the oscillation frequency, $V_{\rm sw}$ is the comparator switching level, $V_{\rm offset}$ is the comparator input offset voltage, C is the total capacitance (i.e., $C_{\rm int}$ + parasitic capacitances), $I_{\rm electrode}$ is the sensor electrode current, $I_{\rm leak}$ is the leakage current (e.g., due to transistor junction leakage) at the circuit nodes connected to the electrode and the comparator input, and $\tau_{\rm delay}$ is the comparator circuit delay time. An approximation for the measured frequency is given by

$$f \approx \frac{I_{\rm sens}}{(V_{\rm sw} \times C)}$$
 (2)

Throughout this paper, the chosen sawtooth amplitude $V_{\rm sw}$ is 1 V and the total capacitance C is approximately 140 fF, so that frequencies are obtained between 7 Hz and 700 kHz for a sensor current range from 10^{-12} A to 10^{-7} A.

The digital part of the pixel circuits consists of two 24-stage counters. Since these counters consume a relatively large portion of the test site area, a design is used which allows to convert the counter circuit into a shift register by a control signal for data readout. Fig. 5(a) and (b) shows one stage of this combined counter/shift register in both operation modes. Inactive parts are shown with thin lines. The circuit consists of two flip-flops and a nMOS network which allows for a very compact layout. In count mode [Fig. 5(a)], the two flip-flops are cross coupled by activating the signal COUNT and deactivating the signals PHI1 and PHI2. In shift mode [Fig. 5(b)], the signal COUNT is set to low, and two nonoverlapping clock signals are used at PHI1 and PHI2 to shift the signal for readout.

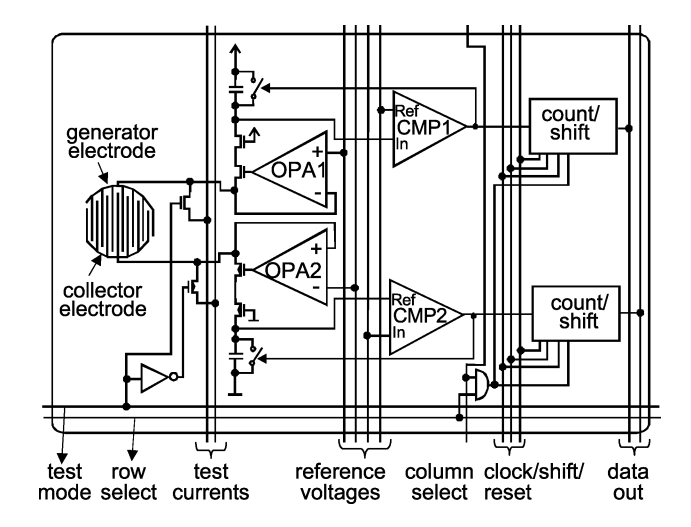


Fig. 6. Complete sensor-site circuit diagram with digital output.

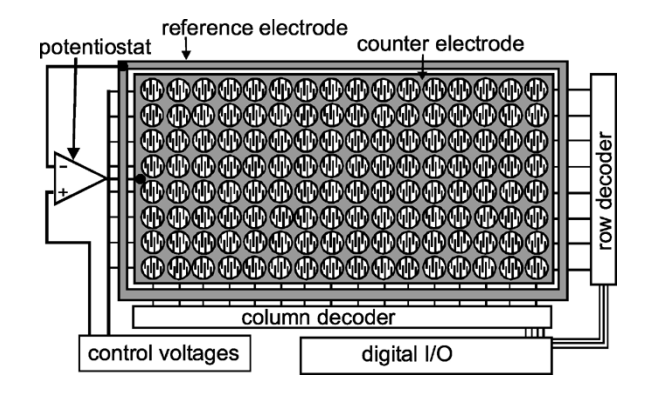


Fig. 7. Chip architecture.

The complete test site circuit is depicted in Fig. 6. It consists of two complementary parts for the generator and collector electrodes, respectively. For calibration or test purposes, direct access to the generator and collector electrodes is available via two transistors.

Fig. 7 shows the overall architecture of the chip. A global potentiostat circuit [25] is used to keep the potential of the electrolyte at a predefined voltage. Row and column decoders are used to select a sensor site for readout.

V. RESULTS AND DISCUSSION

The chip is realized in a 6'' n-well 0.5- μ m CMOS process with two poly and two metal layers, high ohmic poly-silicon resistors, and poly-poly capacitors. Gate oxide thickness is 15 nm, and supply voltage is 5 V. After standard CMOS processing, the gold electrodes are fabricated in a lift-off process after evaporation of a Ti/Pt/Au stack with layer thicknesses of 50 nm/50 nm/500 nm, respectively. Fig. 8 shows a tilted SEM cross section with sensor finger electrodes and CMOS elements after the complete process run. Specific annealing steps are introduced to guarantee both, good electronic CMOS frontend properties and good sensor properties in the process backend [10], [26]. Fig. 9 shows a chip microphotograph of a fully processed sensor array chip with 16×8 positions. The total chip size is $6.4 \text{ mm} \times 4.5 \text{ mm}$.

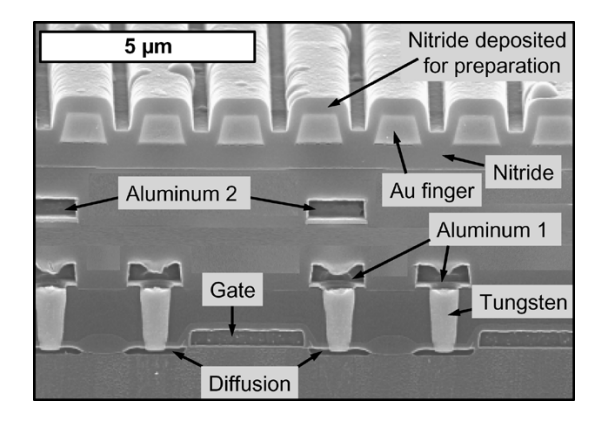


Fig. 8. SEM cross section of the chip.

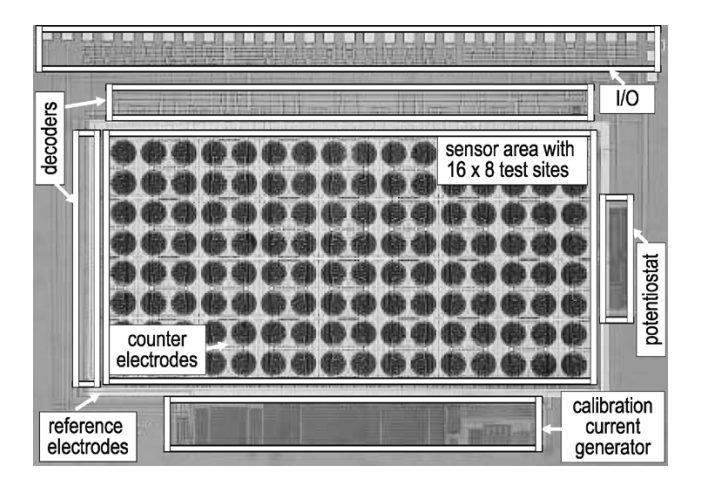


Fig. 9. Chip microphotograph. Total dimensions are 6.4×4.5 mm².

A. Electrical Characterization

The electrical behavior of the chip is characterized for a specified range of currents between 1 pA and 100 nA in a test operation mode. These currents are forced into the circuits via the test inputs using an external current source.

Fig. 10 shows the measured count rate versus input current for all 128 sensor positions from a single chip. Approximately a linear relation between sensor current and frequency is obtained. The measured count rate of 7.2 counts/(pAs) is in good agreement with the design value of 140 fF for the integrating capacitors and 1 V for the sawtooth generator voltage swing. In the current range above 10 nA saturation effects occur which result from frequency limitations of the comparator circuits. This is shown in more detail in Fig. 11, where the relative deviation of the count rate compared to a linear relation, $2 \times (f_{\text{measured}} - f_{\text{calc}}) / (f_{\text{measured}} + f_{\text{calc}})$, with f_{calc} given by (2), is shown as a function of the test current. Three different regions can be distinguished. In the central region between 10^{-11} A and 10^{-8} A, all pixel circuits follow the simple linear relation given by (2) with deviations below 5%. In the region above 10^{-8} A, the frequency increase with increasing current is lower for two reasons. First, a part of the current is systematically not considered since the related charge is not integrated during the time of the reset pulse [$t_{\rm delav}$ in Fig. 3

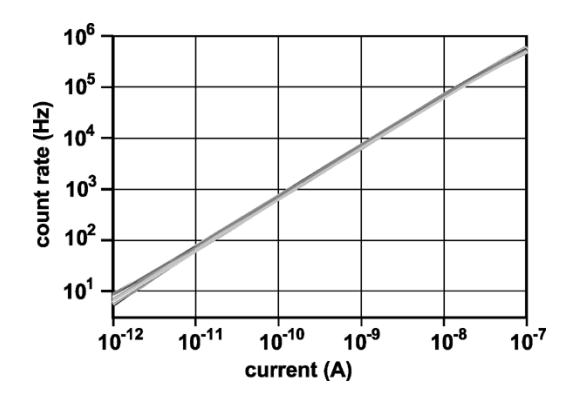


Fig. 10. Measured count rate of all 128 sensor positions versus input current.

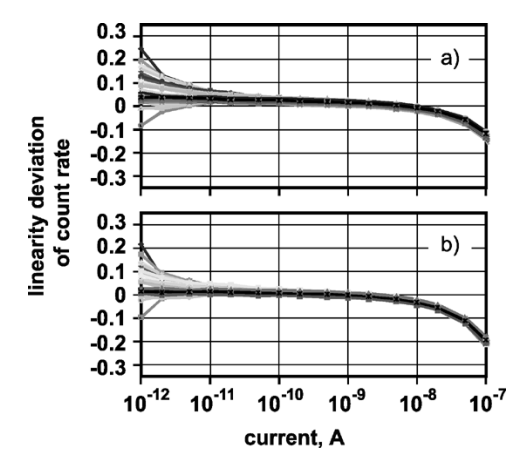


Fig. 11. Linearity deviation of the count rate of the sensor array versus input current, generator electrodes. (a): Comparator type A. (b): Comparator type B.

and (1), respectively]. Second, the delay of the comparator circuits limits the maximum frequency. These effects are more pronounced for comparator type B, since this comparator is slower than the comparator with inverter chain (type A). These effects are well understood by simulations, and a correction of the measured data can easily be done by the readout software. Moreover, in the high current region, range extension can easily be implemented by optionally shunting the integration capacitor with a second device with a 10-fold or 100-fold value, so that the achieved frequencies are lowered by one or two decades. At low current levels (below 10⁻¹¹ A) leakages of the transistors in the current paths lead to a statistically varying behavior of the individual pixel circuits.

The absolute accuracy of the conversion circuits is mainly determined by process variations of the integrating capacitor and the input offset of the comparator. From the specifications of the CMOS process an absolute accuracy better than 5% is estimated, which is more than sufficient for application of such sensor arrays. The more important feature is the homogeneity (i.e., the relative accuracy) of the array. To evaluate this parameter, the standard deviations of the measured frequencies in Fig. 11 are plotted in Fig. 12. As can be seen, the 3σ values are below 2% in the current range from 10^{-10} A to 2×10^{-8} A. In the range from 10^{-11} A to 10^{-7} A, the 3σ variations are below 6%. At 10^{-12} A, the maximum 3σ value is obtained with 20%.

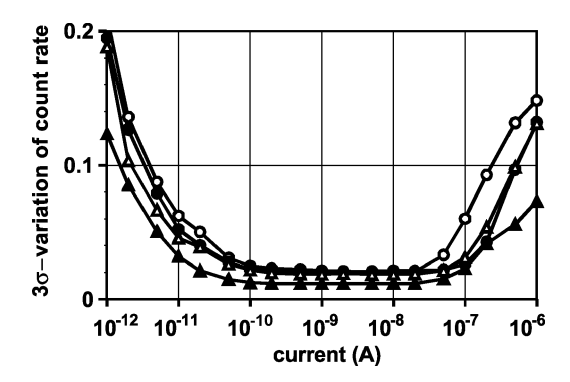


Fig. 12. Homogeneity of the sensor array. Circles: collector circuits, triangles: generator circuits. Full symbols: comparator type A; open symbols: comparator type B.

The shape of the standard deviation as a function of the sensor current can easily be understood using the Gaussian formula for error propagation

$$\sigma^{2}(F(p_{1}, p_{2}, p_{3}, \cdots)) = \sum_{i} \left[\left(\frac{\partial F}{\partial p_{i}} \right)^{2} \times \sigma^{2}(p_{i}) \right]. \quad (3)$$

Applying this relation to (1), the relative standard deviation of the measured frequency is obtained:

$$\begin{split} &\frac{\sigma(f)}{f} \approx \\ &\sqrt{\frac{\sigma^2(I_{\text{leak}})}{I_{\text{electrode}}^2} + \frac{\sigma^2(V_{\text{offset}})}{V_{\text{sw}}^2} + \frac{\sigma^2(C)}{C^2} + \sigma^2(t_{\text{delay}}) \times \left(\frac{I_{\text{electrode}}}{V_{\text{sw}} \times C}\right)^2}. \end{split}$$
(4)

In the mid frequency (resp. mid current range), the variations are dominated by the current- and frequency-independent terms in (4), i.e., by variations of the total capacitance and by the comparator offset voltage. For low currents (resp. low frequencies), leakage current variations lead to a contribution proportional to $1/I_{\rm electrode}$. In the high current (resp. high frequency) region the delay variations dominate due to the fact that the contribution of this parameter increases in proportion to $I_{\rm electrode}$.

In conclusion, the data from Fig. 12 represent tolerable levels for most applications without calibration at a high dynamic range. In case higher accuracy is needed, calibration of the individual pixels via the test ports (see Fig. 6) can be performed to compensate for device parameter variations independent of their origin [9].

B. Electrochemical and Biological Characterization

For an evaluation of the electrochemical sensitivity, the chip is operated with a fluidic cell. Fig. 13 shows the sensor response, when various concentrations of an aqueous para-aminophenol (p-AP) solution are subsequently pumped over the chip. The voltages for the collector and generator electrode are set to -200 mV and +200 mV, respectively. The p-AP is solved in a buffer solution of tris buffered saline (TBS) with pH = 8.5. After each step the flow is stopped. After a short time, the redox cycling process reaches an equilibrium state and approximately equal absolute currents are observed at both electrodes. The levels of the sensor currents correlate reasonably with the

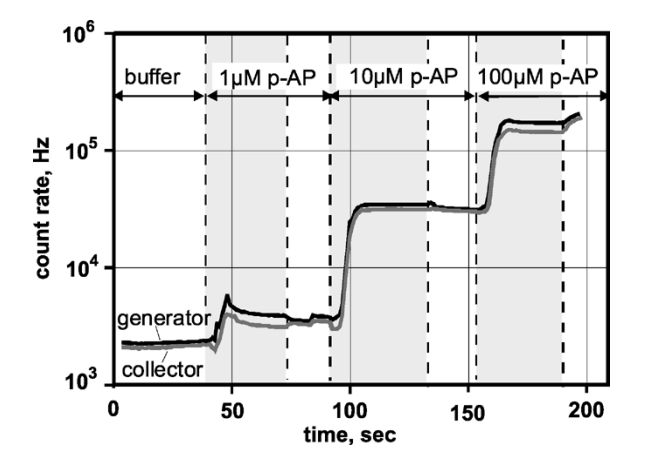


Fig. 13. Measured response of the sensor at various concentrations of para-aminophenole (p-AP). Upper trace: generator current; lower trace: collector current. Gray areas: pump running.

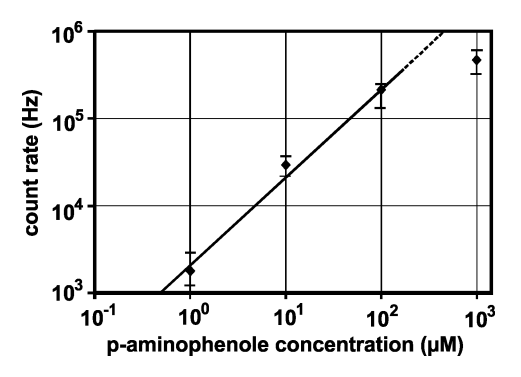


Fig. 14. Measured response of the sensor versus p-AP concentration.

concentration of the redox species (Fig. 14). The straight line shows a linear relation between concentration and sensor current. At high concentrations, electrochemical saturation effects are observed. Optimization of the electrochemical operation conditions promise increased exploitation of the full dynamic electrical range of the circuit.

In order to demonstrate biological functionality, two sensor rows are functionalized with DNA probe sequences with a contact printer. Two different 5'-thiol modified 24-mer probe sequences are spotted on different positions of the sensor array. Immobilization is performed for 60 minutes at room temperature. After immobilization, the surface is washed and blocked with BSA (bovine serum albumin) to reduce the background signal from nonspecific bindings of target molecules to the chip's surface. For hybridization, a 5'-biotin modified 24-mer target sequence is used, which is complementary to one of the immobilized probe sequences. Hybridization is performed for 30 minutes at room temperature. After a washing step, the enzyme complex is added (Alcaline Phosphatase conjugate), which binds to the biotin binding site of the hybridized target molecules. After another washing step, the chip is placed into the measurement flow cell. A flow cell is used in this experiment which covers 5 columns and 16 rows of the sensor field, so that only 80 positions out of 128 are measured. The chip is flooded with para-aminophenylphosphate and the sensor signal is observed after the flow is stopped. Fig. 15 shows the measured count rate versus time for five of the matching

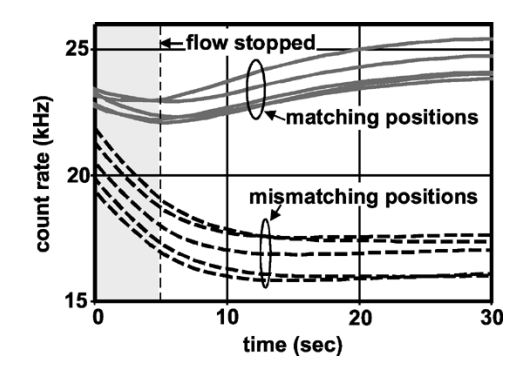


Fig. 15. Sensor response versus time.

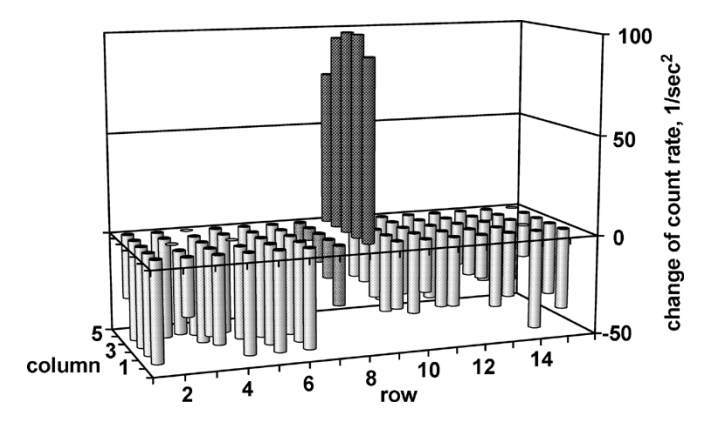


Fig. 16. DNA experiment. Row 8: matching probes, row 7: mismatching probes, all other positions not functionalized.

(row 8) and mismatching (row 7) positions. As can bee seen, the positions with matching and mismatching sequences can clearly be distinguished. In Fig. 16, the current change after the flow stop is shown for 5 rows and 16 columns of the chip. A clear increase in count rate is observed at the matching positions (row 8), whereas no response is seen at the nonmatching positions (row 7) as compared to the uncovered positions. The bell-shaped gradient in the column direction originates from microfluidic nonidealities of the flow cell.

VI. CONCLUSION

A DNA detection chip with 128 positions and fully electronic digital readout has been presented. The sensor site circuit with A/D converted output signals provides a robust data transmission within the array. Moreover, it allows to sample the data from all sites simultaneously which is in particular advantageous for chips with a large number of test sites. The chip allows a wide dynamic range of five decades and provides a homogeneity of the sensor response better than 20% in the current range from 10^{-12} A to 10^{-7} A and better than 6% in the range from 10^{-11} A to 10^{-7} A. The electrochemical and biological function of the chip has been demonstrated.

REFERENCES

[1] E. M. Southern, "An improved method for transferring nucleotides from electrophoresis strips to thin layers of ion-exchange cellulose," *Anal. Biochem.*, vol. 62, no. 1, pp. 317–318, Nov. 1974.

- [2] M. Schena, Ed., DNA Microarrays: A Practical Approach. Oxford, U.K.: Oxford University Press, 2000.
- [3] M. Schena, Ed., Microarray Biochip Technology. Natick, MA: Eaton Publishing, 2000.
- [4] D. Meldrum, "Automation for genomics, sequencers, microarrays, and future trends," *Genome Research*, vol. 10, pp. 1288–1303, 2000.
- [5] F. Bier and J. P. Fürste, "Nucleic acid based sensors," in *Frontiers in Biosensorics I*, F. Schubert, F. W. Scheller, and J. Fedrowitz, Eds. Basel, Switzerland: Birkhäuser Verlag, 1997.
- [6] T. Vo-Dinh and B. Cullum, "Biosensors and biochips: advances in biological and medical diagnostics," *Fresenius J. Anal. Chem.*, vol. 366, pp. 540–551, 2000.
- [7] P. Hegde, R. Qi, K. Abernathy, C. Gay, S. Dharap, R. Gaspard, J. E. Hughes, E. Snesrud, N. Lee, and J. Quackenbush, "A concise guide to cDNA microarray analysis," *Biotechniques*, vol. 29, no. 3, pp. 548–556, 2000
- [8] M. Xu, J. Li, Z. Lu, C. Feng, Z. Zhang, P. K. Ko, and M. Chan, "A high density conduction based micro-DNA-identification array fabricated in a CMOS compatible process," in *IEEE ISSCC Dig. Tech. Papers*, 2003, pp. 198–199.
- [9] R. Thewes, F. Hofmann, A. Frey, B. Holzapfl, M. Schienle, C. Paulus, P. Schindler, G. Eckstein, C. Kassel, M. Stanzel, R. Hintsche, E. Nebling, J. Albers, J. Hassman, J. Schülein, W. Goemann, and W. Gumbrecht, "Sensor arrays for fully electronic DNA detection on CMOS," in *IEEE ISSCC Dig. Tech. Papers*, 2002, pp. 350–351.
- [10] F. Hofmann, A. Frey, B. Holzapfl, M. Schienle, C. Paulus, P. Schindler-Bauer, D. Kuhlmeier, J. Krause, R. Hintsche, E. Nebling, J. Albers, W. Gumbrecht, K. Plehnert, G. Eckstein, and R. Thewes, "Fully electronic DNA detection on a CMOS chip: device and process issues," in *IEDM Tech. Dig.*, 2002, pp. 488–491.
- [11] R. Hintsche, M. Paeschke, A. Uhlig, and R. Seitz, "Microbiosensors using electrodes made in Si-technology," in *Frontiers in Biosensorics*, F. Schubert, F. W. Scheller, and J. Fedrowitz, Eds. Basel, Switzerland: Birkhäuser Verlag, 1997, p. 267.
- [12] M. Schienle, A. Frey, F. Hofmann, B. Holzapfl, C. Paulus, P. Schindler-Bauer, and R. Thewes, "A fully electronic DNA sensor with 128 positions and in-pixel A/D conversion," in *IEEE ISSCC Dig. Tech. Papers*, 2004, pp. 220–221.
- [13] E. Zubritsky, "Spotting a microarray system," Anal. Chem., vol. 72, no. 23, pp. 761A–767A, 2000.
- [14] M. J. Heller, "An active microelectronics device for multiplex DNA analysis," *IEEE Eng. Med. Biol. Mag.*, pp. 100–104, 1996.
- [15] S. P. A. Fodor, R. P. Rava, X. C. Huang, A. C. Pease, C. P. Holmes, and C. L. Adams, "Multiplexed biochemical assays with biological chips," *Nature*, vol. 364, pp. 555–556, 1993.
- [16] GeneChip arrays, reagents, instruments, and software. Affymetrix. [On-line]. Available: http://www.affymetrix.com
- [17] K. Dill, D. Montgomery, W. Wang, and J. Tsai, "Antigen detection using microelectrode array microchips," *Analytica Chimica Acta*, vol. 444, pp. 69–78, 2001.
- [18] A. J. Bard, J. A. Crayston, G. P. Kittlesen, T. V. Shea, and M. S. Wrighton, "Digital simulation of the measured response of reversible redox couples at microelectrode arrays: consequences arising from closely spaced ultramicroelectrodes," *Anal. Chem.*, vol. 58, pp. 2321–2331, 1986.
- [19] A. J. Bard and L. R. Faulkner, *Electrochemical Methods*. New York: Wiley, 2001.
- [20] M. Paeschke, U. Wollenberger, C. Köhler, T. Lisec, U. Schnakenberg, and R. Hintsche, "Properties of interdigital electrode arrays with different geometries," *Analytica Chimica Acta*, vol. 305, pp. 126–136, 1995.
- [21] S. Kleinfelder, L. Suki-Iwan, L. Xinquiao, and A. El Gamal, "A 10 kframe 0.18 μm CMOS digital pixel sensor with pixel-level memory," in *IEEE ISSCC Dig. Tech. Papers*, 2001, pp. 88–89.
- [22] W. Yang, "A wide-dynamic-range, low-power photosensor array," in IEEE ISSCC Dig. Tech. Papers, 1994, pp. 230–231.
- [23] U. Ringh, C. Jansson, C. Svensson, and K. Liddiard, "CMOS RC-oscillator technique for digital read out from an IR bolometer array," in *Int. Conf. Solid-State Sensors and Actuators Tech. Dig.*, 1995, pp. 138–141.
- [24] K. Tanaka, F. Ando, K. Taketoshi, I. Ohishi, and G. Asari, "Novel digital photosensor cell in GaAs IC using conversion of light intensity to pulse frequency," *Jpn. J. Appl. Phys.*, vol. 32, pp. 5002–5007, Nov. 1993.
- [25] A. Frey, M. Jenkner, M. Schienle, C. Paulus, B. Holzapfl, P. Schindler-Bauer, F. Hofmann, D. Kuhlmeier, J. Krause, J. Albers, W. Gumbrecht, D. Schmitt-Landsiedel, and R. Thewes, "Design of an integrated potentiostat circuit for CMOS bio sensor chips," in *Proc. ISCAS*, vol. V, 2003, pp. 9–12.

[26] A. Frey, F. Hofmann, R. Peters, B. Holzapfl, M. Schienle, C. Paulus, P. Schindler-Bauer, D. Kuhlmeier, J. Krause, G. Eckstein, and R. Thewes, "Yield evaluation of gold sensor electrodes used for fully electronic DNA detection arrays on CMOS," *Microelectron. Reliabil.*, vol. 42, pp. 1801–1806, 2002.



Meinrad Schienle received the Dipl. Phys. and Ph.D. degrees from the University of Karlsruhe, Germany, in 1979 and 1983, respectively.

In 1984, he joined the Research Laboratories of Siemens AG, working on integrated optical components based on III/V semiconductors. Since 1999, he has been with Corporate Research, Infineon Technologies AG, Munich, Germany, working on design-based yield evaluation and circuit design for flash memories. He is currently working on the development of fully electronic DNA sensors.



Christian Paulus received the diploma degree in physics from the University of Bayreuth, Germany, in 1997. He is currently working toward the Ph.D. degree at the University of Magdeburg, Germany.

Since 1997, he has been with Siemens AG, Corporate Technology, Munich, Germany, and Infineon Technologies AG, Corporate Research, Munich. He is working in the field of CMOS-based biosensors and advanced analog circuits.



Birgit Holzapfi graduated from the Engineering School of Siemens AG, Munich, Germany.

In 1983, she joined the Siemens Research Laboratory. From 1983 to 1985, she worked on the development of surface acoustic wave filters, and from 1986 to 1998, on research projects concerning GaAs hetereostructure devices and on the evaluation of the matching behavior of silicon devices, respectively. Since 1999, she has been with Corporate Research at Infineon, Munich, where she is involved in the design of CMOS-based biosensors.



After a six months period working in industrial proteomic research, she joined the Few Electron

Circuits group at Infineon's Corporate Research, Munich, Germany, in 2000. Presently, she is working on the development of fully electronic DNA sensors.

 $\mbox{Dr.}$ Schindler-Bauer is a member of the technical program committee of the IEEE Sensors Conference.



peripheral circuits.

Alexander Frey was born in Jena, Germany, in 1970. He received the M.A. degree from the University of Texas, Austin, in 1994, and the Dipl. Phys. degree from the Justus-Maximilian-Universitaet Wuerzburg, Germany, in 1997.

Since 1997, he has been with the Research Laboratories of Siemens AG and Infineon Technologies, Munich, Germany. He was engaged in the design for gigabit DRAM sensing circuits. Currently, his interests lie in the design of electrochemical sensing and biasing circuits for biosensors and system related



Roland Thewes (M'99) was born in Marl, Germany, in 1962. He received the Dipl.-Ing. degree and the Dr.-Ing. degree in electrical engineering from the University of Dortmund, Germany, in 1990 and 1995, respectively.

From 1990 to 1995, he worked in a cooperative program between the Siemens Research Laboratories in Munich and the University of Dortmund in the field of hot-carrier degradation in analog CMOS circuits. Since 1994, he has been with the Research Laboratories of Siemens AG and Infineon

Technologies, where he was active in the design of nonvolatile memories and in the field of reliability and yield of analog CMOS circuits. From 1997 to 1999, he managed projects in the fields of design for manufacturability, reliability, analog device performance, and analog circuit design. Since 2000, he has been responsible for the Laboratory on Few Electron Circuits of Corporate Research of Infineon Technologies. His current interests include electronic biosensors on CMOS, device physics-related circuit design, and advanced analog CMOS circuit design. He has authored or co-authored some 90 publications, including two book chapters.

Dr. Thewes has served as a member of the technical program committees of the International Reliability Physics Symposium (IRPS), and of the European Symposium on Reliability of Electron Devices, Failure Physics and Analysis (ESREF). He is a member of the technical program committees of the International Solid-State Circuits Conference (ISSCC), of the International Electron Device Meeting (IEDM), and of the European Solid State Device Research Conference (ESSDERC). In 2004, he joined the IEEE EDS VLSI Technology and Circuits Committee. He is a member of the German Association of Electrical Engineers (VDE).



Franz Hofmann joined the Corporate Research Laboratories of Siemens AG in Munich in 1986. He was involved in the development of the 16 Mbit and the 64 Mbit DRAM. Since 1993, he has been engaged in the research of novel devices and memory cells using vertical transistors. From this research, a high density ROM with vertical transistors and a two-fold density compared to a planar cell was developed. In 1999, he joined Infineon Corporate Research where he worked on surrounding gate transistors which can be used in the DRAM generation below-90-nm fea-

ture size. Since 2001, he has been engaged in silicon process development for novel sensors in the biological field. He holds more than 50 patents on semiconductor devices for DRAM, nonvolatile memory cells, and biological sensors.